Au@ZrO₂ Hollow Fiber Catalytic Membrane for CO Preferential Oxidation in Hydrogen-Rich Gas with High Stability and Efficiency

Feng Zhu,[†] Yuting Zhang,[†] Xuehong Gu,*,[†] Changlin Chen,[†] Wanqin Jin,[†] and Xuebin Ke[‡]

[†]State Key Laboratory of Materials-Oriented Chemical Engineering, College of Chemistry and Chemical Engineering, Nanjing Tech University, 5 Xinmofan Road, Nanjing 210009, P. R. China

[‡]School of Chemistry, Physics and Mechanical Engineering, Faculty of Science and Engineering, Queensland University of Technology, Brisbane QLD4001, Australia

Supporting Information Placeholder

ABSTRACT: CO preferential oxidation (CO-PROX) is of much interest as a way to remove the trace CO in reformed gases and utilize hydrogen. Herein, we investigate the use of gold nano-particles embedded in uniform hollow fiber ZrO₂ membranes for CO elimination in the presence of hydrogen. The flow-through catalytic membrane exhibited higher catalytic activity (above 96%) than conventional catalyst pellets and retain long-term stability up to 110 hours. The high catalytic performance combined with its outstanding stability suggests the developed Au@ZrO₂ catalytic membrane as a promising candidate for the removal of CO.

Hydrogen, as a green energy carrier derived from fossil fuels or biofuels, has been greatly attractive in last decades. Proton exchange membrane fuel cell (PEMFC) supplied with hydrogen is by far the most advanced power generation device for its high energy conversion efficiency, rapid start-up, and low operating temperature. It always requires an ultra-low CO content of <100 ppm to prevent Pt anode from poisoning. CO preferential oxidation (CO-PROX) in H₂-rich gas is a critical reaction for CO deep elimination.[1] Since Haruta et al.[2] discovered that small gold nano-particles finely dispersed on certain metal oxide supports can exhibit surprisingly high activity for CO oxidation below room temperature, extensive and intensive studies have addressed the structures and mechanisms associated with gold catalysts.[3,4,5] The size of the gold nano-particles and the support properties have been shown to be critical to their unique catalytic activity.[3] Due to the low melting point (1336 K) and weak binding energy of gold, however, small gold nano-particles tend to be aggregated, forming larger gold particles upon calcination, which causes poor dispersion and low catalytic activity. Up to now, great efforts have been made on design, characterization, and activation of gold catalysts.[4]

Gold nano-particles have been found to possess high activities at low temperature (i.e., <120 °C) when supported on reducible oxides,[5] such as TiO₂, CeO₂, and Fe₂O₃. Recent progress showed that ZrO₂ supported gold nano-particles exhibited quite active for CO oxidation.[6] However, Konova et al.[7] observed that the deactivation on Au/ZrO₂ catalyst, attributed to the formation of carbonates. It is possible that the generated CO₂ in the catalyst is favourable to form carbonates during CO-PROX reaction and block the active sites. Therefore, immediate removal of the produced CO₂ would be helpful to hinder the formation and accumulation of carbonates.

Herein, we developed a novel Au@ZrO₂ hollow fiber catalytic membrane with high stability and efficiency. It is presented for CO-PROX in a flow-through catalytic membrane reactor (FTCMR). Feeding stream is driven through catalytic membrane layer, which presents many advantages compared with conventional packed-bed reactor. The flowing stream could sweep the generated CO₂ and thus improve catalytic stability; the catalytic performance could be further enhanced by intensive contact between reactants and active sites of catalysts; the advantages in recovery, regeneration, and reuse of catalysts in successive processes, are remarkable.[8] Improved activity on Pt-loaded zeolite membranes has been observed for CO-PROX operated at 200 °C.[9]
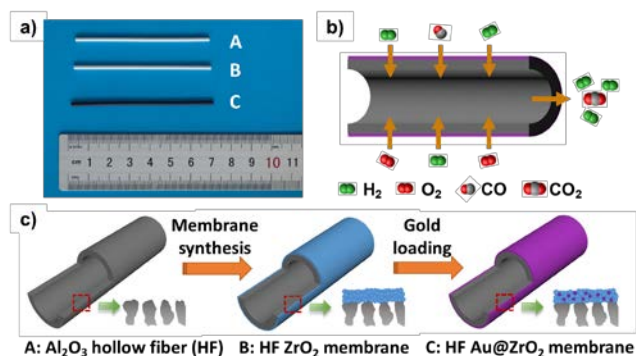

Figure 1. a) Photographs of the Al₂O₃ hollow fiber, ZrO₂ membrane and Au@ZrO₂ membrane; schematic representation of b) CO-PROX reaction carried out using the catalytic membrane; c) preparation procedure of hollow fiber Au@ZrO₂ membrane.

Herein, both catalytic activity and stability of Au@ZrO₂ catalytic membranes are crucial for gold catalyst in practical applications. Moreover, hollow fiber configured membranes

with small diameters were used to load gold catalyst, which could provide a high membrane area/volume ratio in membrane modules during scaled-up processes (e.g. tubes, 30-250 m²/m³; multi-channel monolithics, 130-400 m²/m³; hollow fibers, >1000 m²/m³).[10]

Figure 1 shows the preparation procedure of Au@ZrO₂ catalytic membrane. Porous α-Al₂O₃ hollow fibers were fabricated by a dry-wet spinning technique.[11] They offered an outer diameter/inner diameter (O.D./I.D.) of 1.8 mm/0.9 mm, an average pore size ~0.65 μm and a porosity about 48%. ZrO₂ membranes were prepared by hydrothermally secondary growth using ZrO₂ particles as seeds. The ZrO₂ seeds with an average particle size around 1.5 μm were ball-milled from original particles (Figure S1a). After dip-coating twice in seeds solution (aqueous solution containing 1 wt% ZrO₂), a seed layer with uniform and good coverage was formed on outer surface of the hollow fiber (Figure S1b). The seeded support was immersed into synthesis solution for hydrothermal crystallization at 180 °C for 60 h. The as-synthesized membrane was then calcined at 450 °C for 4 h. It can be seen from Figure S1c-d that a close-packing ZrO₂ membrane with regular thickness of about 10 μm was grown on the outer surface of the hollow fiber. For loading gold nano-particles, the ZrO₂ membrane was immersed in 1.2 mM HAuCl₄ solution adjusted at pH = 9.0 with 0.5 M NH₄OH under stirring for 12 h at 80 °C, and then washed with deionized water until it was free of chloride ions. N₂ adsorption isotherms are given in Figure S2. The Au@ZrO₂ membrane exhibits a smaller surface area (64.4 m²/g) and pore size (9.7 nm) than ZrO₂ membrane due to the gold nano-particles embedded in ZrO₂ pores.
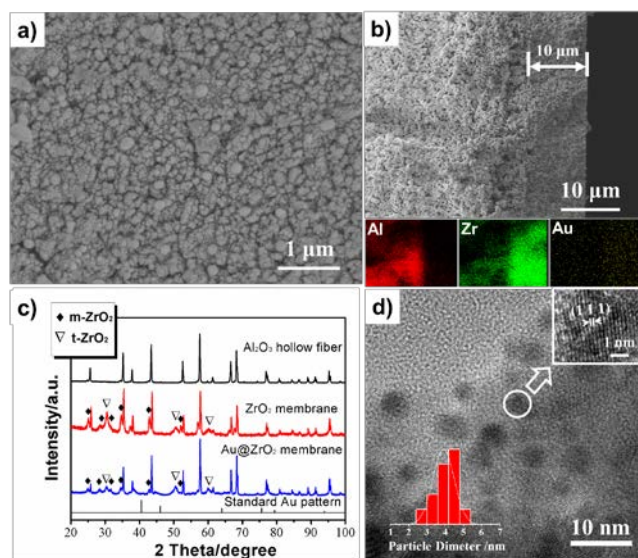

Figure 2. (a) Surface of Au@ZrO₂ membrane; (b) SEM-EDX mapping images of cross-section of Au@ZrO₂ membrane; (c) XRD patterns of Al₂O₃ hollow fiber, ZrO₂ membrane and Au@ZrO₂ membrane; (d) TEM of the Au@ZrO₂ membrane before reaction. Inset: HRTEM image of the selected areas.

Figure 2a displays SEM image for surface of a hollow fiber Au/ZrO₂ catalytic membrane, which exhibited similar morphology to the membrane before gold loading. Figure 2b shows SEM image for cross-section of the catalytic membrane with EDX mapping results. The distribution of Al, Au and Zr elements were associated with Al₂O₃ hollow fiber support and catalytic membrane layer separately. We can observe that a few amounts of Au and Zr were penetrated into Al₂O₃ support during membrane synthesis; however, the bulk of catalyst was located on the membrane layer. XRD patterns show that ZrO₂ membrane consists of monoclinic-type and tetragonal-type crystalline structures (Figure 2c). We did not observe the reflection peaks associated with gold, indicating the nano-sized gold particles dispersed well in the porous ZrO₂ membranes. But we scratched off some fragments from the membrane surface for high-resolution transmission electron microscopy (HRTEM) analysis. Figure 2d shows the HRTEM image of the membrane fragments. It can be seen that gold particles with average diameter of 3.3 nm were dispersed in ZrO₂ membranes uniformly. The gold particles were nearly spherical and The spacing between lattice fringes was 0.23 nm, corresponding to the (1 1 1) planes of the face-centered cubic (fcc) Au (Figure 2d inset).
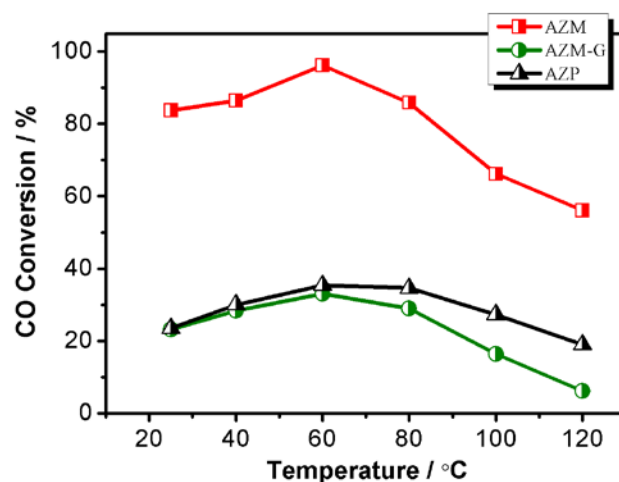

Figure 3. CO-PROX conversion profiles vs. temperature of Au/ZrO₂ catalytic membranes (AZM), (AZM-G) and catalyst pellets(AZP). Reaction conditions: CO 0.67%, O₂ 1.33%, H₂ 32.67%, He balance (vol. %). GHSV = 18,000 h⁻¹

A hollow fiber Au@ZrO₂ catalytic membrane (marked as AZM) was used to evaluate reaction performance of CO-PROX. The membrane had an active length of 7.5 cm and total weight of 0.373 g with gold loading of 0.37 wt%. For comparison, Au/ZrO₂ particles (fabricated by hydrothermally synthesized ZrO₂ particles, marked as AZP) and the pellets from ground catalytic membrane (marked as AZM-G) were packed in a conventional fixed-bed reactor for CO-PROX. The gold amounts of AZP and AZM-G for reaction were the same as that of AZM. Figure 3 shows the reaction results for AZM, AZP and AZM-G. The catalytic activity tests were performed at 105 kPa between 25 °C and 120 °C. As can be seen, CO conversion increased with temperature before 60 °C for the three reactions, which was due to the increasing catalytic activity at elevated reaction temperature. When the operating temperature was higher than 60 °C, CO conversion decreased with temperature due to competitive H₂ oxidation. It was interesting to observe that AZM exhibited ultra-high CO conversion than the conventional reactors, either AZM-G or AZP. Typically, at 60 °C, CO conversion of 96.2% was achieved in the membrane reactor AZM, while the CO conversions were only 33.0% and 35.4% in AZM-G and AZP, re-

spectively. As shown in Figure S3, O_2 selectivity decreased with the operating temperature for the three reactions, which was a typical tendency for gold catalysts. It has been found that low temperature is favourable to CO oxidation as competing with H_2 oxidation. There was no obvious difference in O_2 selectivity at 25 °C of 100% for AZM, AZM-G and AZP. However, AZM showed relatively higher O_2 selectivity than AZM-G and AZP at high operating temperature. The results suggested that intensive contact between reactants and gold active sites by flow-through membrane reactor were highly effective to improve CO conversion for CO-PROX. Due to faster diffusion of H_2 through micro channels than CO, CO molecules would have longer resident time in catalytic system, which is beneficial to O_2 selectivity.

Table 1. Comparison of TOFs over AZM, AZM-G and AZP at 60 °C.

Sample	Au loads /wt%	CO conversion/%	TOF/s^{-1}
AZM	0.37	96.2	4.73
AZM-G	0.37	33.0	1.62
AZP	2.61	35.4	2.06

Turnover frequency (TOF) was calculated for the purpose of performance comparison in Table 1. Here, TOF is moles of CO converted per second divided by the total moles of gold atoms and described in more detail in the Supporting Information. The AZM gave a TOF of 4.73 s^{-1} at 60 °C exhibiting significantly higher catalytic activity than AZM-G and AZP. A detailed TOF comparison between our AZM and gold catalysts reported in literatures can be found in Table S1. As shown in the table, the AZM appears to be the most active one among gold-based catalysts reported so far.

A fresh AZM was used for long-term stability test, as shown in Figure 4. For the first stage, AZM was operated in a feeding stream containing 0.67% CO, 1.33% O_2 and 32.67% H_2 balanced with He. It was found that stable CO conversion up to 100% was achieved during the first 110 h (stage A). Since the practical feed gas for PEMFC always contains CO_2 and H_2O, it is important to know CO_2 and H_2O tolerances of the Au@ZrO$_2$ catalytic membrane. Therefore, 25% CO_2 was added into the feeding stream (CO 0.50%, O_2 1.0%, H_2 24.50%, CO_2 25%, He balance) on stage B for CO-PROX. As shown in Figure 4, CO conversion dropped about 6% after the addition of CO_2. It is interesting to find that CO conversion could be stable in CO_2 atmosphere during 48 h operation. After shutting off CO_2 stream, the conversion could be partially recovered and maintained at about 97% in the next 90 h (stage C). Konova et al.[7] synthesized high surface area ZrO$_2$ for Au/ZrO$_2$ catalysts by hydrolysis of ZrCl$_4$; the conversion of the obtained catalysts decreased dramatically about 65% after 500 minutes. Ilieva et al.[12] observed that high concentration of CO_2 drastically decreased activities of some supported gold catalysts. Schubert et al.[5e] studied the effects of CO_2 on PROX by means of FTIR for Au/a-Fe$_2$O$_3$; they found the addition of CO_2 reduced the CO conversion and the deactivation was accelerated due to the blocking effect of carbonate formation on active sites. Similar opinions were also held by other researchers.[4d, 7] In this work, the results indicated excellent durability of Au@ZrO$_2$ catalytic membranes under CO_2 atmosphere. The limited decreases in CO conversion

could be attributed to the refreshment of continuous flowing stream by reducing the resident time of CO and CO_2 to avoid formation of carbonates. On stage D, we further introduced H_2O into feeding stream (CO 0.67%, O_2 1.33%, H_2 32.67%, H_2O 10.5%, He balance) at the same reaction temperature. It was noticed that the CO conversion immediately declined to about 10%. The addition of H_2O leads to the blocking of active sites by adsorbed H_2O molecules at low temperature.[13] When raising the temperature to 120 °C (stage E-F), the CO conversion increased accordingly due to reduced H_2O adsorption. It was interesting to find that the CO conversion increased largely after shutting off H_2O addition (stage F), possibly due to H_2O desorption on active sites. When the temperature returned to 60 °C (stage G), the activity of the membrane was continuously recovered and the CO conversion maintained around 95% during 400-hour operation.
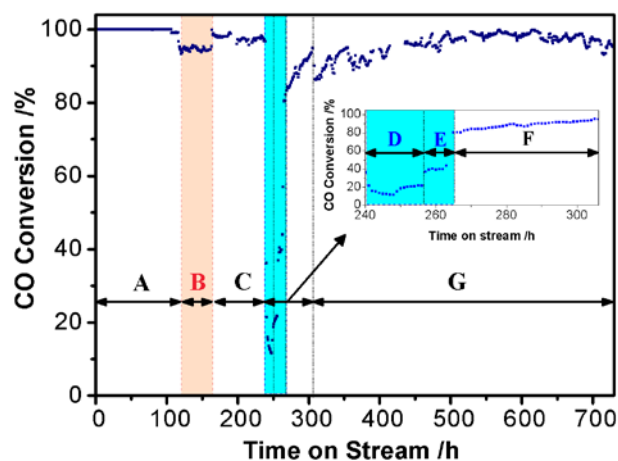

Figure 4. Long-term stability test for CO-PROX conversion over AZM. Reaction conditions: (A, C, G) CO 0.67%, O_2 1.33%, H_2 32.67%, He balance, 60 °C. (B) CO 0.50%, O_2 1.00%, H_2 24.50%, CO_2 25.00%, He balance, 60 °C. (D) CO 0.67%, O_2 1.33%, H_2 32.67%, H_2O 10.5%, He balance, 60 °C. (E) CO 0.67%, O_2 1.33%, H_2 32.67%, H_2O 10.5%, He balance, 120 °C. (F) CO 0.67%, O_2 1.33%, H_2 32.67%, He balance, 120 °C.

We wondered whether the flow-through membrane reactor made an important contribution to the stability. Therefore, the stabilities of an Au@ZrO$_2$ catalytic membrane and Au/ZrO$_2$ particle were further compared. The feeding stream was a mixture of 0.67% CO, 1.33% O_2 and 32.67% H_2 balanced with He with GHSV of 18,000 h^{-1}, which produced an initial CO conversion less than 100% for both reactors. In this way, we can clearly evaluate the activity with operation time. As can be seen from Figure S4, CO conversion over AZM was stable at about 94% and no apparent activity loss was found in 100 h. Comparatively, AZP showed a stable CO conversion of 26% during first 40 h and then gradually decreased to about 17% after that. High-angle annular dark-field scanning transmission electron microscopy (HAADF-STEM) observation from Figure S5a-b shows that the small gold nanoparticles were still well dispersed in AZM after CO PROX reaction. Little gold agglomeration was seen in both AZM and AZP after CO PROX reaction (Figure S5c-d). We speculated the decrease in CO conversion was a result of carbonates formation, which can be effectively inhibited by the

flowing stream in membrane reactor to immediately remove CO_2 and unreacted CO.

To further understand the effect of carbonate species on the stability of AZM and AZP, X-ray photoelectron spectroscopy (XPS) measurements were taken before and after CO PROX reactions. An analysis of the corresponding C1s peaks, Figure S6, pointed out the formation of carbonates on the surface of the catalysts. C1s spectra of AZM (Figure S6a-b), recorded before and after PROX reactions shows peaks at 284.8, 286.5, which is due to ubiquitous carbon C-C and C-O. The shoulder peak at 288.8 eV is attributed to C=O.[14] In the case of AZP (Figure S6c-d), the spectra before reaction is similar with that of AZM. After reaction, the shoulder peaks at 289.4 eV and 292.4 eV are expected to result from the accumulation of carbonate or bicarbonate species on AZP.[15] The resultant carbonates would remain on the catalyst surface and the accumulation of such species leads to the deactivation of catalytic activity.[16]

In summary, we have successfully prepared gold nanoparticles embedded in a hollow fiber ZrO_2 membrane for CO PROX reaction. The resulting Au@ZrO_2 catalytic membrane exhibited an exceptionally higher activity than its ground pellets or Au/ZrO_2 particle enhanced by intensive contact between reactants and active sites. Such catalytic performance is better than the conventional gold-based catalysts. The catalytic membrane exhibits long-term stability which has great potential in practical application for removal of CO in H_2 as demanded by PEMFC. These results show the feasibility of employing this kind of catalytic membrane in broader contexts, such as ammonia synthesis, hydrogenation process. Moreover, the hollow fiber configured membranes could provide high packing density that is necessary for fabrication of compact modules. Further research is being focused on the correlation between the membrane structure and catalytic performance.

ASSOCIATED CONTENT

Supporting Information

List of papers describing synthesis routes of hollow fiber Au@ZrO_2 membranes; morphologies of ZrO_2 membranes; N_2 adsorption isotherms; O_2 selectivity profiles vs. temperature; long term stability tests over AZM and AZP; TEM images; XPS spectras; comparison of TOFs; and more experimental details. This material is available free of charge via the Internet at http://pubs.acs.org.

AUTHOR INFORMATION

Corresponding Author

*Xuehonggu@yahoo.com
Notes
The authors declare no competing financial interest.

ACKNOWLEDGMENT

REFERENCES

(1) (a) Kahlich, M. J.; Gasteiger, H. A.; Behm, R. J. *J. Catal.*, **1999**, 182, 430. (b) Park, E. D.; Lee, D.; Lee, H.C. *Catal. Today*, **2009**, 139, 280. (c) Schubert, M. M.; Plzak, V.; Garche, J.; Behm, R. J. *Catal. Lett.*, **2001**, 76, 143.

(2) (a) Haruta, M.; Kobayashi, T.; Sano, H.; Yamada, N. *Chem. Lett.*, **1987**, 16, 405. (b) Haruta, M.; Yamada, N.; Kobayashi, T.; Iijima, S., *J. Catal.*, **1989**, 115, 301. (c) Haruta, M. *Nature*, **2005**, 437, 1098.

(3) (a) Vaidyanathan, S.; Eduardo, E. W.; Prashant, V. K. *J. Am. Chem. Soc.*, **2004**, 126, 4943. (b) Dong, C. L.; Ignacio, L. S.; Rainer, D.; Moritz, B.; Young, D. K.; *Angew. Chem. Int. Ed.*, **2006**, 45, 2413. (c) Valden, M.; Lai, X.; Goodman, D. W. *Science*, **1998**, 281, 1647. (d) Alexis, T. B. *Science*, **2003**, 299, 1688. (e) Green, I. X.; Tang, W.; Neurock, M.; Yates, J. T., *Science*, **2011**, 333, 736. (f) Liu, X. Y.; Wang, A. Q.; Zhang, T.; Mou, C. Y. *Nano Today*, **2013**, 8, 403.

(4) (a) Gong, J. L.; *Chem. Rev.*, **2012**, 112, 2987. (b) Guo, Z.; Liu, B.; Zhang, Q. H.; Deng, W. P.; Wang, Y.; Yang, Y. H., *Chem. Soc. Rev.*, **2014**, 43, 3480. (c) Xu, C. X.; Su, J. X.; Xu, X. H.; Liu, P. P.; Zhao, H. J.; Tian, F.; Ding, Y. *J. Am. Chem. Soc.*, **2007**, 129, 42. (d) Kung, H. H.; Kung, M. C.; Costello, C. K.. *J. Catal.*, **2003**, 216, 425. (e) Chen, M. S.; Goodman, D. W. *Catal. Today*, **2006**, 111, 22. (f) Zhu, H. Y.; Ke, X. B.; Yang, X. Z.; Sarina S.; Liu, H. W. *Angew. Chem.*, **2010**, 122, 9851. (g) Lin, Q. Q.; Qiao, B. T.; Huang, Y. Q.; Li, L.; Lin, J.; Liu, X. Y.; Wang, A. Q.; Li, W. C.; Zhang, T. *Chem. Commun.*, **2014**, 50, 2721.

(5) (a) Chen, M. S.; Goodman, D. W. *Science*, **2004**, 306, 252. (b) Lee, S.; Fan, C. Y.; Wu, T. P.; Scott L. A.. *J. Am. Chem. Soc.*, **2004**, 126, 5682. (c) Kim, H. Y.; Lee, H. M.; Graeme, H. *J. Am. Chem. Soc.*, **2012**, 134, 1560. (d) Zhang, C. J.; Angelos, M.; Stephen J. J. *Phys. Chem. Chem. Phys.*, **2011**, 13, 22. (e) Schubert, M. M.; Venugopal, A.; Kahlich, M. J.; Plzak, V.; Behm, R. J. *J. Catal.*, **2004**, 222, 32. (f) Philip, L.; Jonathan, F.; Benjamin, E. S.; Tomas, G.; Saleh, A. S.; Albert, F. C.; Andrew, A. H.; Christopher, J. K.; Michiel, M.; Jacob, A. M.; Arjan, O.; Stanislaw, E. G.; Graham J. H. *J. Mater. Chem.*, **2006**, 16, 199. (g) Philip, L.; Jonathan, F.; Benjamin, E. S.; Tomas, G.; Albert, F. C.; Andrew, A. H.; Christopher, J. K.; Stanislaw, E. G.; Graham, J. H. *Chem. Commun.*, **2005**, 27, 3385. (h) Zhao, K. F.; Qiao, B. T.; Wang, J. H.; Zhang, Y. J.; Zhang, T. *Chem. Commun.*, **2011**, 47, 1779.

(6) (a) Comotti, M.; Li, W. C.; Spliethoff, B.; Schuth, F. *J. Am. Chem. Soc.*, **2006**, 128, 917. (b) Arrii, S.; Morfin, F.; Renouprez, A. J.; Rousset, J. L. *J. Am. Chem. Soc.*, **2004**, 126, 1199.

(7) Konova, P.; Naydenov, A.; Tabakova, T.; Mehandjiev, D. *Cata. Comm.*, **2004**, 5, 537.

(8) Marcano, J. G. S.; Theodore, T. T. *Catalytic membranes and membrane reactors.* Wiley-VCH Verlag GmbH, **2002**.

(9) (a) Bernardo, P.; Algieri, C.; Barbieri, G.; Drioli, E. *Catal. Today*, **2006**, 118, 90. (b) Bernardo, P.; Algieri, C.; Barbieri, G.; Drioli, E. *Sep. Purif. Technol.*, **2008**, 62, 629.

(10) Li Jiansheng; Wang Lianjun; Hao Yanxia; Liu Xiaodong; Sun Xiuyun. *J. Membr. Sci.*, **2005**, 256 1.

(11) (a) Chen, Y. Y.; Shi, Z. Z.; Zhang, C.; Gu, X. H.. *J. Inorg. Mater.*, **2014**, 29, 143. (b) Luiten-Olieman, M. W. J.; Winnubst, L.; Nijmeijer, A.; Wessling, M.; Benes, N. E. *J. Membr. Sci.*, **2011**, 370, 124.

(12) Lyuba, I.; Giuseppe, P.; Ivan, I.; Rodolfo, Z.; Janusz, W. S.; Wojciech L.; Anna M. V.; Donka A. *Catal. Today*, **2011**, 175, 411.

(13) Fujitani, T.; Nakamura, I.; Haruta, M. *Catal. Lett.*, **2014**, 144, 1475.

(14) (a) Afzal, A.; Di Franco, C.; Mesto, E.; Ditaranto, N.; Cioffi, N.; Scordari, F.; Torsi, L. *Mater. Express*, **2015**, 5, 171. (b) Igal, D.; Moshe, M.; Stas, O.; Reuven, B.; Gitti, L. F. *J. Mater. Chem. A*, **2014**, 2, 16746

(15) (a) Wang, H.; Zhu, H.; Qin, Z.; Liang, F.; Wang, G.; Wang, J. *J. Cata.*, **2009**, 264, 154. (b) Kast, P.; Kučerová, G.; Behm, R. J. *Cata. Today*, **2015**, 244, 146. (c) de Smit, E.; van Schooneveld, M. M.; Cinquini, F.; Bluhm, H.; Sautet, P.; de Groot, F. M.; Weckhuysen, B. M. *Angew. Chem.*, **2011**, 123, 1622.

(16) (a) Okumura, M.; Tsubota, S.; Haruta, M. *Angew. Chem. Int. Ed.*, **2004**, 43, 2129. (b) Romero-Sarria, F.; Domínguez, M. I.; Centeno, M. A.; Odriozola, J. A. *Appl. Cata. B: Environ.*, **2011**, 107, 268. (c) del Río, E.; Collins, S. E.; Aguirre, A.; Chen, X.; Delgado, J. J.; Calvino, J. J.; Bernal, S. *J. Catal.*, **2014**, 316, 210-218.

Catalytic Membrane for CO Preferential Oxidation in Hydrogen-rich Gas with High Stability and Efficiency

Feng Zhu,[†] Yuting Zhang,[†] Xuehong Gu*,[†], Changlin Chen,[†] Wanqin Jin,[†] and Xuebin Ke[‡]

[†]State Key Laboratory of Materials-Oriented Chemical Engineering, College of Chemistry and Chemical Engineering, Nanjing Tech University, 5 Xinmofan Road, Nanjing 210009, P. R. China.

[‡]School of Chemistry, Physics and Mechanical Engineering, Faculty of Science and Engineering, Queensland University of Technology, Brisbane QLD4001, Australia.

*Corresponding author: Tel.: +86-25-8317-2268, E-mail: Xuehonggu@yahoo.com (X. Gu)

1. Experimental Section

1.1 Preparation of α-Al$_2$O$_3$ hollow fiber substrates

Al$_2$O$_3$ hollow fibers were prepared by a dry-wet spinning technique. α-Al$_2$O$_3$ powders (d_{50} = 0.8 μm, Hai-Gang-Hua-Tai functional ceramics Co., Ltd.), polyethersulfone (PESf, BD-5, Bei-Shi-De synthetic plastics company), N-methyl-2-pyrrolidone (NMP, AR, Sinopharm Chemical Reagent Co., Ltd.) and polyvinylpyrrolidone (PVP, K-30, AR, Sinopharm Chemical Reagent Co., Ltd.) were used as the fiber material, binder, solvent and additive, respectively. The spinning suspension had a mass ratio of α-Al$_2$O$_3$: PESf: NMP: PVP = 49.7:9.94:39.83:0.53. After degassing, the spinning suspension was pressurized by compressed nitrogen. The spinning process was carried out by extruding the suspension through a single-bore spinneret into an external coagulant used with tap water. The air gap was kept at 10 cm for all spinning runs. The extrusion rate of the suspension and the flow rate of the internal coagulant (deionized water) were kept at 1.3~1.5 m min^{-1} and 40 mL s^{-1}, respectively. The hollow fiber precursors were left in the external coagulant overnight for complete solidification. After having dried, the hollow fibers were sintered at 1450 °C for 5 h.

1.2 Preparation of ZrO$_2$ seeds

7g zirconium (IV) nitrate tahydrate (Zr(NO$_3$)$_4$·5H$_2$O, ≥99.5%, AR, Sinopharm Chemical Reagent Co., Ltd) was added into 100 mL deionized water and dissolved adequately. The pH of this aqueous solution was then adjusted to 9.0 by 0.5 M NH$_4$OH solution while the solution was being stirred. After aged for 12 h and freeze-dried for 24 h, the initial ZrO$_2$ powders were collected. The ZrO$_2$ seeds were obtained by ball-milling ZrO$_2$ powders for 6 h using a planetary ball mill (PM-100, Retsch. Ind. Ltd) with zirconium oxide balls as grinding media.

1.3 Preparation of hollow fiber ZrO$_2$ membranes

Al$_2$O$_3$ hollow fiber substrates were firstly ultrasonically cleaned in deionized water and then dried in an oven at 60 °C. Both ends of hollow fibers were wrapped by Teflon tapes. The substrates were dipped into an aqueous seed suspension with seeds content of 1 wt% for 10 s (dip-coating) and dried at 60 °C. This process was repeated twice. Subsequently the seeded substrates were sintered at 450 °C for 4 h.

The synthesis gel for ZrO$_2$ membranes were prepared from the Zr(NO$_3$)$_4$ solution pre-adjusted to pH = 9. The seeded substrates were immersed in the precursor solution and hydrothermally synthesized at 180 °C for 60 h. The ZrO$_2$ membranes were obtained after calcined at 450 °C for 4 h in air.

1.4 Gold loading on ZrO$_2$ membranes

A HAuCl$_4$ stock solution was prepared by dissolving 1.0 g of HAuCl$_4$·4H$_2$O (Shanghai Reagent, Shanghai, China) in 200 mL of deionized water and was stored at 4 °C. Hollow fiber ZrO$_2$ membranes were immersed in 1.2 mM HAuCl$_4$ solution pre-adjusted to pH=9.0 by 0.5 M NH$_4$OH solution. The aqueous solution was stirred at 80 °C for 12 h. Extensive washing with deionized water was then followed until it was free of chloride ions. The samples were dried at 60 °C for 12 h, and calcined at 300 °C for 3 h in air.

1.5 Characterizations

Particle size analysis was conducted using a Malvern ZS90 zeta-sizer. The as-made ZrO$_2$ powders were dispersed in deionized water to obtain a suspension and all measurements were conducted at 25 °C.

The crystal phases were characterized by powder X-ray diffraction were (XRD, Rigaku MiniFlex 600) with a Cu-Kα radiation source in the 2θ range of 20°-100°.

The morphologies of the resultant materials were observed by field-emission scanning electron microscopy (FESEM, Hitachi S-4800). The FESEM instrument was equipped with an energy-dispersive X-ray analysis (EDX, EMAX x-act, Horiba), which was used to identify the elemental compositions of the catalytic membranes.

Transmission electron microscopy (TEM) and High-angle annular dark-field scanning transmission electron microscopy (HAADF-STEM) images were obtained with a Tecnai G2 F30 S-Twin transmission electron microscope operating at an accelerating voltage of 200 kV.

Nitrogen sorption studies, surface area and pore size distribution were obtained by Brunauer–Emmett–Teller (BET) method on powdered samples at a bath temperature of 77.3 K using Micromeritics surface area analyzer (ASAP-2020)

X-ray photoelectron spectroscopy (XPS) measurements were performed with a ESCALAB 250X spectrometer equipped with a monochromatic Al X-ray source (1486.6 eV) (ThermoElectron Co., America). The base pressure in the analysis chamber was 1×10^{-10} mbar. The binding energy scale was corrected using the C 1s signal located at 284.8 eV.

The specific gas adsorption behaviours of the membranes were obtained by adsorption experiments at 25 °C (ASAP 2020, Micromeritics, USA)

1.6 CO preferential oxidation

The activity of a hollow fiber Au/ZrO_2 catalytic membrane was evaluated by CO preferential oxidation. Prior to reaction, the Au/ZrO_2 catalytic membrane was activated at 300 °C in H_2 flow for 1 h. The feed was a mixture of 0.67% CO, 1.33% O_2 and 32.67% H_2 balanced with He (vol. %). GHSV = 18,000 h^{-1}. The reaction was conducted at different temperature from 25 °C to 120 °C. The GC injections for gas analysis for every reactor used in this study were repeated three times to obtain more reliable results. In the long-term stability test, CO_2 was added into feed stream from 120 h to 160 h with 25 vol. % and the effect of water vapour was also tested by passing the gas feed through a ''water bubbler'' in front of the reactor with H_2O addition of 10.5 vol. %.

The CO conversion was calculated, respectively, by:

$$X_{CO} = \frac{F_{CO}^{Feed} - F_{CO}^{Outlet}}{F_{CO}^{Feed}} \qquad (1)$$

The selectivity of O_2 is defined as the ratio of O_2 that reacted with CO to the total consumption:

$$S_{O_2} = \frac{0.5(F_{CO}^{Feed} - F_{CO}^{Outlet})}{F_{O_2}^{Feed} - F_{O_2}^{Outlet}} \qquad (2)$$

The turnover frequency was calculated as:

$$TOF = \frac{F_{CO}^{Feed} \cdot X_{CO} \cdot M_{Au}}{m_{cat} \cdot Au_{wt.\%} \cdot D} \ (s^{-1}) \qquad (3)$$

The turnover frequencies (TOF) were calculated on the basis of the number of Au atoms exposed at the surfaces, which were estimated from the mean diameters and actual loadings of the Au particles. In this calculation, the shape of Au particles was assumed to be closed-shell particles of nearly spherical shape. Where F_{CO}^{Feed} is the molar flow rate of CO in feed stream, mol s^{-1}. F_{CO}^{Outlet} is the molar flow rate of CO in outlet stream, mol s^{-1}. $F_{O_2}^{Feed}$ is the molar flow rate of O_2 in feed stream, mol s^{-1}. $F_{O_2}^{Outlet}$ is the molar flow rate of O_2 in outlet stream, mol s^{-1}. X_{CO} is the conversion of CO at 60 °C, %. M_{Au} is the gold atom weight, 197 g mol^{-1}. m_{cat} is the mass of the $Au@ZrO_2$ catalytic membrane, g, $Au_{wt.\%}$ is the weight percent of gold in the catalytic membrane, %. D is the gold dispersion ($Au_{surface}/Au_{total}$) calculated from the average size of gold nanoparticles d_{Au} (nm) according to D = 1.168/d_{Au}, %.

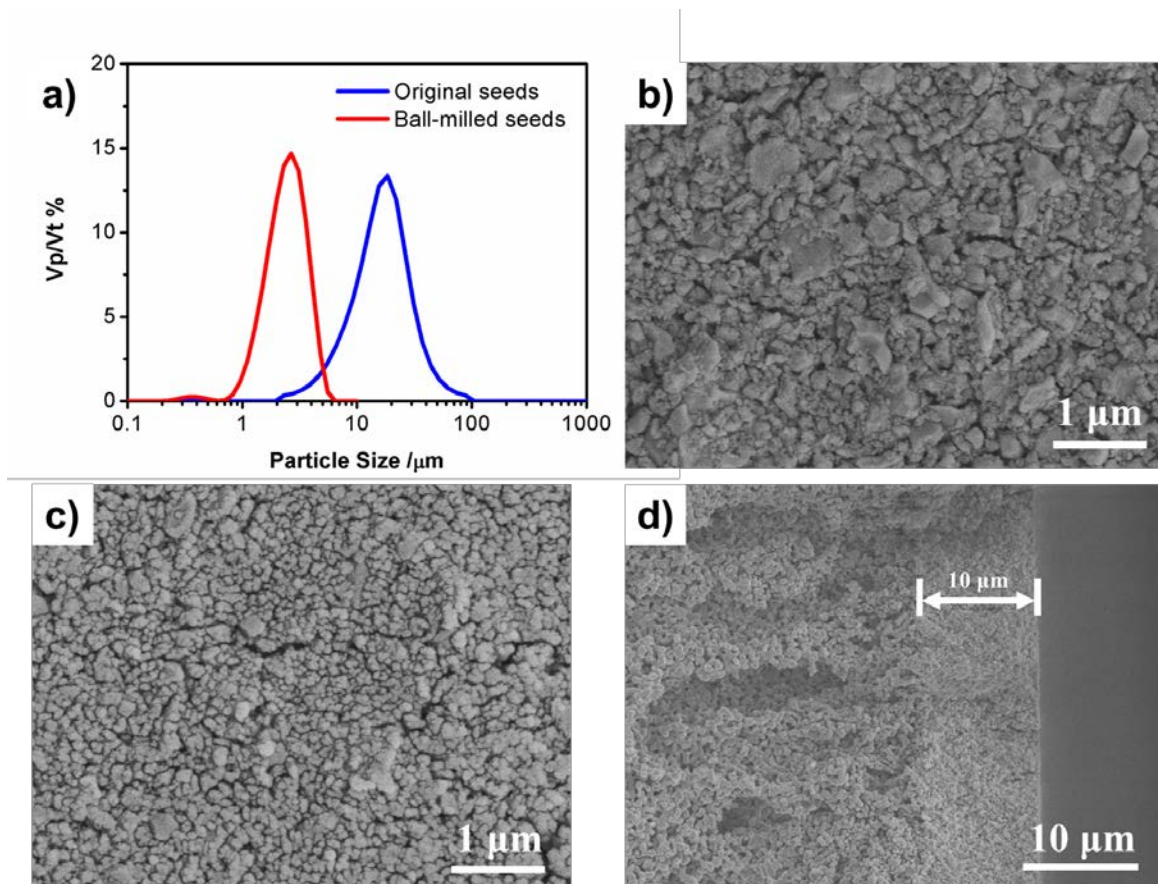## 2. Supporting Notes

Figure S1

Figure S1. (a) Particle size distributions of the ZrO_2 seeds before and after ball-milling treatment; SEM images: (b) Surface of ball-milled ZrO_2 seeded support; (c) Surface and (d) cross section of ZrO_2 membrane.
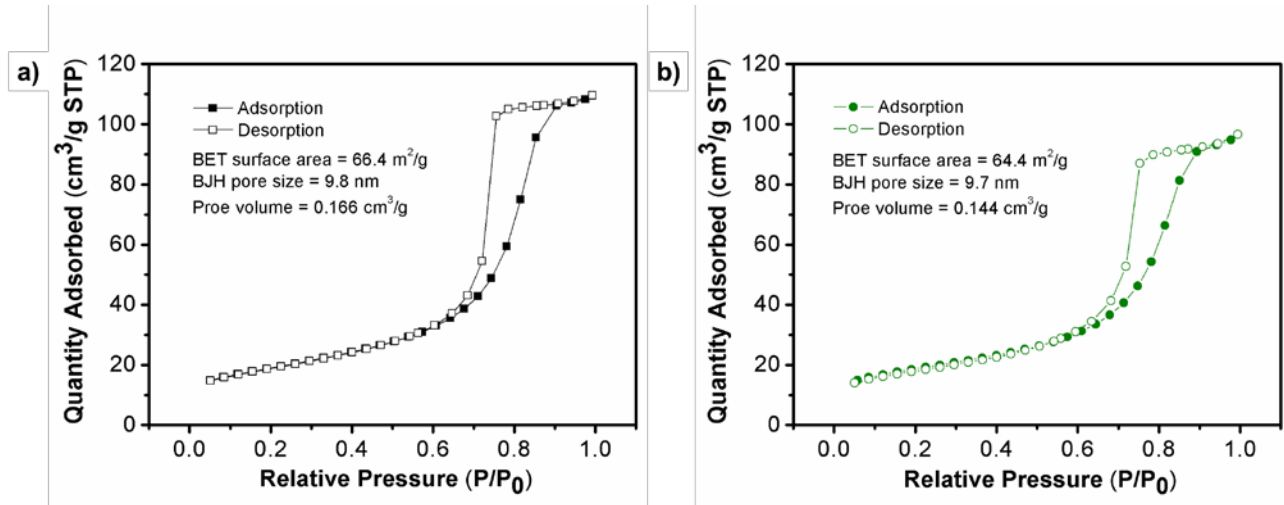
Figure S2

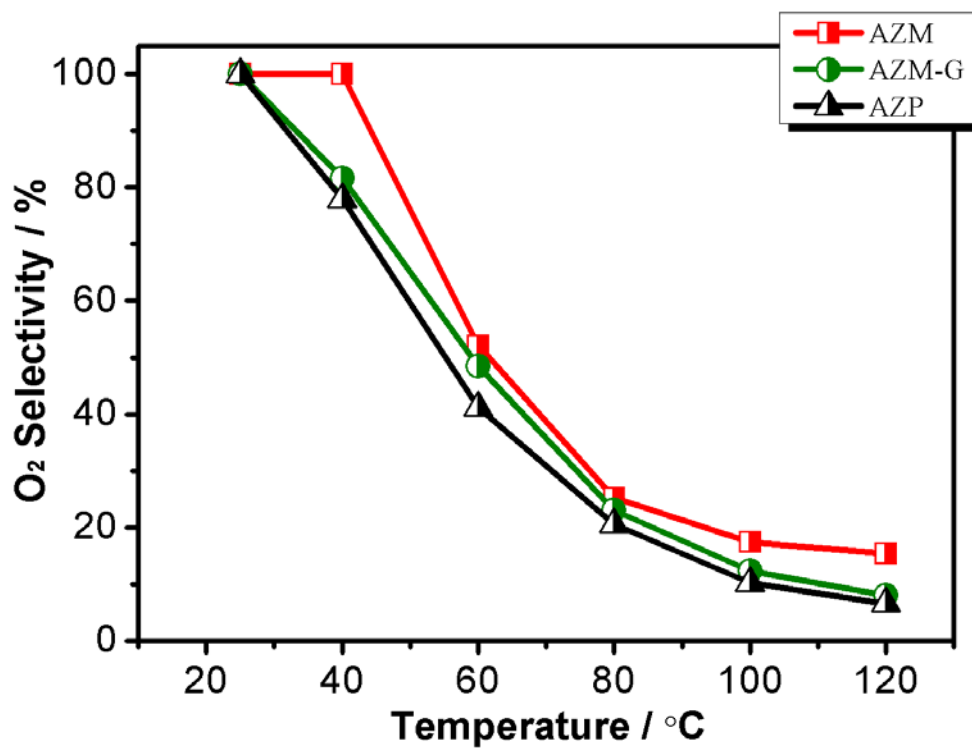Figure S2. N$_2$ adsorption isotherms of (a) ZrO$_2$ membrane and (b) Au@ZrO$_2$ membrane.

Figure S3. O_2 selectivity profiles vs. temperature of AZM, AZM-G and AZP. Reaction conditions: CO 0.67%, O_2 1.33%, H_2 32.67%, He balance (vol. %). GHSV = 18,000 h^{-1}
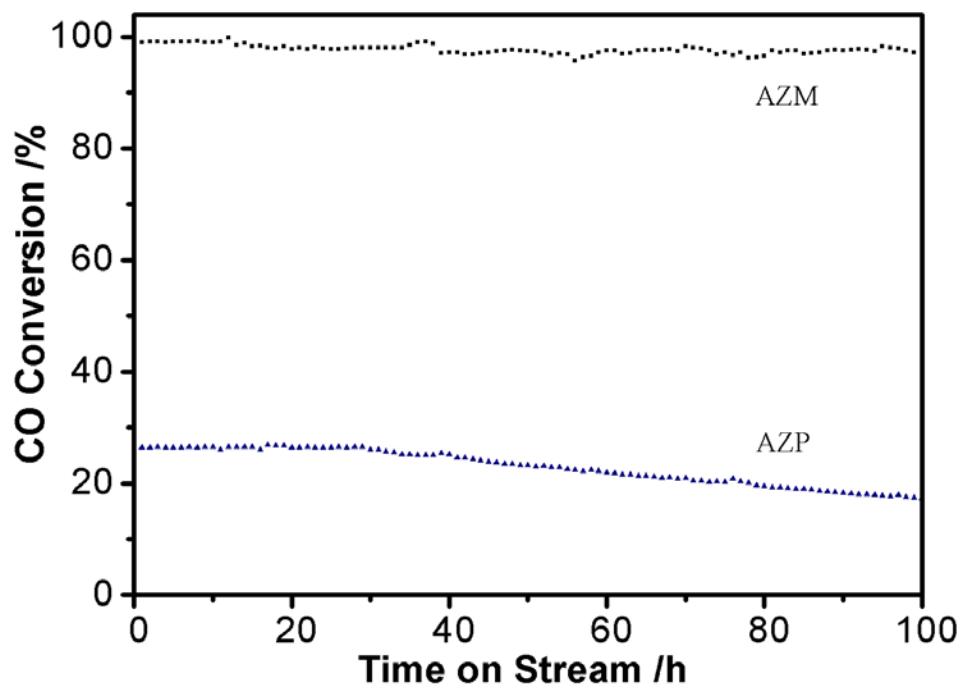
Figure S4. Long term stability tests for CO-PROX conversion over AZM and AZP. Reaction conditions: CO 0.67%, O_2 1.33%, H_2 32.67%, He balance (vol. %). GHSV = 18,000 h^{-1}
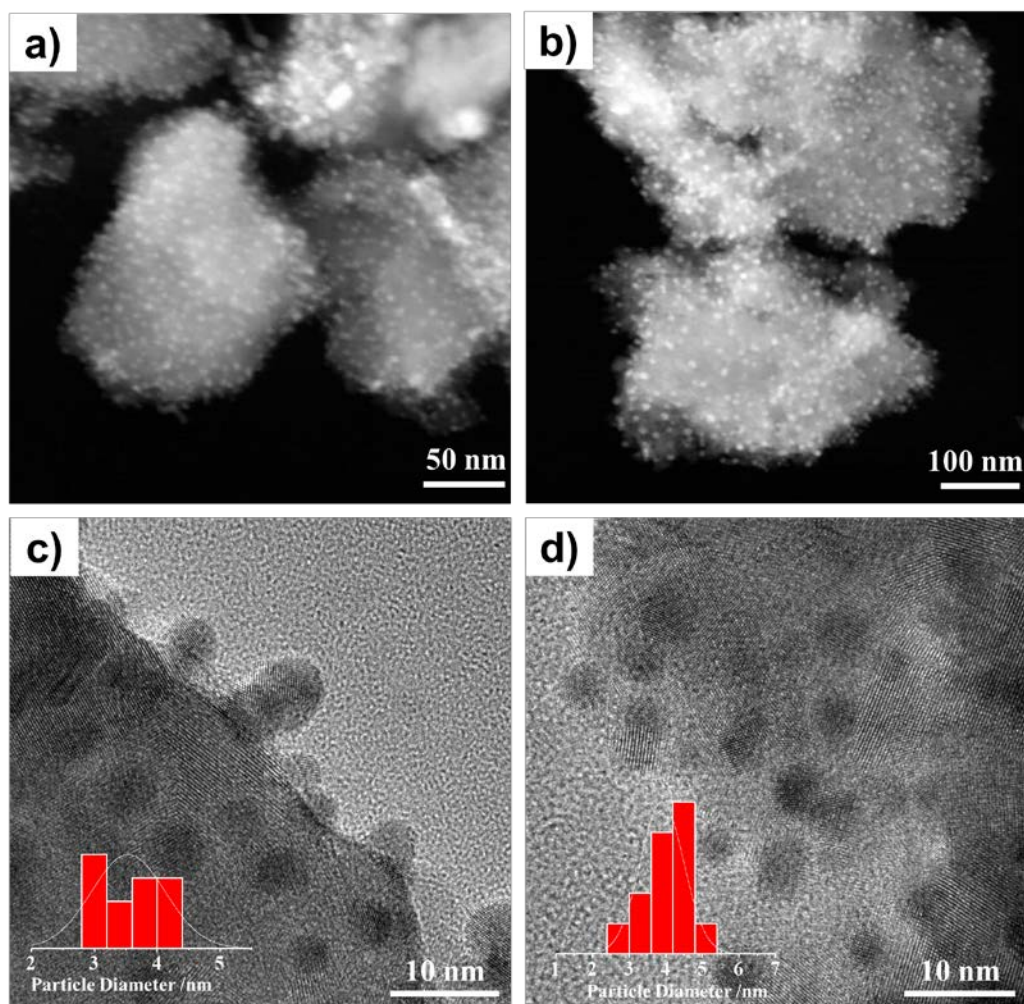
Figure S5. HAADF-STEM images of the AZM (a) before and (b) after reaction; TEM images of (c) AZM and (d) AZP after reaction.
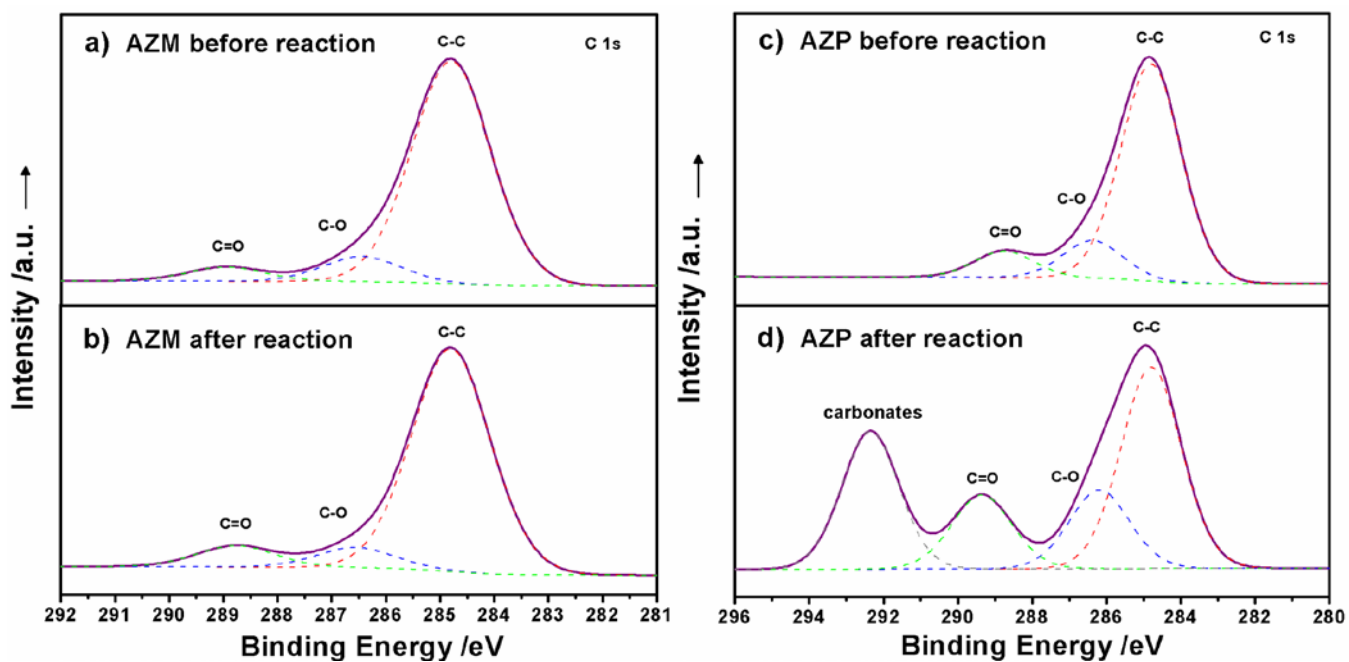
Figure S6. XPS C1s spectras for AZM a) before b) after reaction and AZP c) before d) after reaction.

Table S1. Comparison of TOFs for CO oxidation over AZM, AZM-G, AZP and literature data.

Reaction system	Particle Size (nm)	Au loading (wt%)	TOF/s^{-1}	Reference
AZM	3.3	0.37	4.73	This work
AZM-G	3.3	0.37	1.62	This work
AZP	3.9	2.61	2.06	This work
Au/TiO$_2$	3.7	1.4	2.8	(1)
Au/α-Fe$_2$O$_3$	3.1	1.1	2.3	(2)
Au/CeO$_2$	2.2	2.24	1.4	(2)
Au/TiO$_2$	2.4	1.77	2.0	(2)
Au/CeO$_2$	1.3	3	0.36	(3)
Au/Mn$_2$O$_3$	2.2	2.9	0.55	(4)
Au/Fe$_2$O$_3$	3.6	0.66	0.086	(5)
Au/Co$_3$O$_4$	~2	1.2	0.48	(5)
Au/TiO$_2$	3	3.3	0.32	(5)

References

1. Elodie Quinet, Laurent Piccolo, Franck Morfin, Priscilla Avenier, Fabrice Diehl, Valérie Caps, Jean-Luc Rousset. J. Catal., 2009, 268, 384.
2. Markus M. Schubert, Vojtech Plzak, Jürgen Garche, R. Jürgen Behm. Catal. Lett., 2001, 76, 143.
3. Titilayo Shodiya, Oliver Schmidt, Wen Peng, Nico Hotz. J. Catal., 2013, 300, 63.
4. Lu-Cun Wang, Qian Liu, Xin-Song Huang, Yong-Mei Liu, Yong Cao, Kang-Nian Fan. Appl. Catal. B: Environ., 2009, 88, 204.
5. M. Haruta, S. Tsubota, T. Kobayoshi, H. Kageyama, M. J. Genet, B. Delmon. J. Catal., 1993, 144, 175.